Noname manuscript No.
(will be inserted by the editor)

Nanoscale origin of the thermo-mechanical behavior of clays

Laurent Brochard · Túlio Honório · Matthieu Vandamme · Michel Bornert · Michael Peigney

Received: date / Accepted: date

Abstract We investigate the physics behind the complex thermo-mechanical behavior of clays. Depending on their loading history, clays exhibit thermal expansion or contraction, reversible or irreversible, and of much larger magnitude than for usual solids. This anomalous behavior is often attributed to water adsorption, but a proper link between adsorption and thermo-mechanics is still needed, which is the object of this paper. We propose a conceptual model starting from the scale of the adsorption up to the scale of the geomaterial, which successfully explains the thermo-mechanical behavior of clays. Adsorption takes place between clay layers at the nanometer scale. The mechanics of the clay layers is known to be strongly affected by adsorption, e.g., swelling with humidity increase. Here we investigate the effect of drained heating and show that an increase of temperature decreases the amplitude of the confining pressure oscillations with the basal spacing. More subtle is a shift of the oscillations to larger basal spacing. To relate the mechanics of a clay layer to that of the geomaterial, we propose an upscaling in two steps: the clay particle and the clay matrix with inclusions. We model the particle as a stack of layers in which different hydration states (number of water layers in a nanopore) can co-exist. This description builds on the theory of shape memory alloys, the physics of which is quite analogous to the case of a clay particle. Upscaling to the scale of the clay matrix with inclusions is performed with conventional self-consistent homogenization. The conceptual model is confronted to three typical experiments of the thermo-mechanical behavior of clay. It captures all the anomalous behaviors of clays: expansion / contraction, reversibility / irreversibility, role of loading history and impact on preconsolidation pressure. Moreover, it offers a possible nanoscale interpretation of each of these anomalous behaviors.

Keywords clays · thermal expansion / contraction · micromechanics · water adsorption

L. Brochard
Laboratoire Navier, UMR 8205, École des Ponts, IFSTTAR, CNRS, UPE, Champs-sur-Marne, France.
E-mail: laurent.brochard@enpc.fr

T. Honório
Laboratoire Navier, UMR 8205, École des Ponts, IFSTTAR, CNRS, UPE, Champs-sur-Marne, France.

M. Vandamme
Laboratoire Navier, UMR 8205, École des Ponts, IFSTTAR, CNRS, UPE, Champs-sur-Marne, France.

M. Bornert
Laboratoire Navier, UMR 8205, École des Ponts, IFSTTAR, CNRS, UPE, Champs-sur-Marne, France.

M. Peigney
Laboratoire Navier, UMR 8205, École des Ponts, IFSTTAR, CNRS, UPE, Champs-sur-Marne, France.

1 Introduction

Clays are geomaterials ubiquitous in sedimentary soils and rocks and are therefore involved in a wide variety of geomechanical applications. For instance, clays usually exhibit low permeability and are thus suitable sealing media for nuclear wastes disposal or caprocks for carbon geological storage. Regarding mechanics, clays exhibit some unusual behaviors such as the well-known swelling with increasing humidity. This mechanical behavior is at the heart of many challenges in geomechanics from foundations design to oil and gas recovery and geothermal energy. A particular issue, which we investigate in this paper, is the thermo-mechanical behavior of clays.

Indeed, many applications involve thermal loadings, notably nuclear waste disposal, which has long motivated studies of the mechanical response of clays to temperature variations. The first studies of thermo-mechanical behavior of clays dates back to the 1960's [42,13,46] and have identified some key features that were confirmed on a wide variety of clays since then. We can summarize these as follows :

- Normally consolidated clays contract irreversibly upon drained heating under constant confining stress. Drained cooling is reversible. This observation leads to the concept of thermal consolidation.
- The irreversible contraction is reduced for over-consolidated clays. Heavily over consolidated clays exhibit first a reversible thermal expansion at low temperatures and then irreversible contraction at higher temperatures.
- The elastic domain is reduced with temperature increase, i.e., preconsolidation pressure decreases with temperature. Moreover, thermal consolidation induces strain hardening. However, temperature has almost no influence on the elastic and plastic compressibilities.
- Apparent drained irreversible thermal contractions are typically $\sim -10^{-3}\mathrm{K}^{-1}$ whereas reversible thermal expansions are typically $\sim 10^{-4}\mathrm{K}^{-1}$. These magnitudes are significantly higher than that of other solids (e.g., $\sim 3\cdot 10^{-5}\mathrm{K}^{-1}$ for steel or concrete) and that measured for the solid mineral constituents of clays : $1.5\cdot 10^{-5}$ to $5.4\cdot 10^{-5}\mathrm{K}^{-1}$ [36].

To clarify and illustrate this thermo-mechanical behavior we display in Figure 1 the results of three typical experiments. In the first experiment (Fig. 1 (a)) volumetric deformations of clay samples upon temperature cycles (20°C to 100°C) are reported. The samples are drained, under constant confining pressure, and differ in over consolidation ratio (OCR) defined as the ratio between the plastic limit and the current confining pressure. These results clearly show that consolidation state is a key property for the thermo-mechanical behavior. Normally consolidated clays (OCR = 1) contract irreversibly upon heating, while over-consolidated clays (OCR > 1) first expand reversibly and then contract irreversibly. The pressure has only little effect on the deformation. The experimental results presented here were obtained by [48] for Boom clay (see also [20]), but similar results have been observed for Pontida silty clay [5], Pasquasia clay [29], kaolin clay [54,16], Bangkok clay [3], bentonite [51] and Opalinus claystone [39]. Accordingly, this behavior can be considered representative of swelling clays in general.

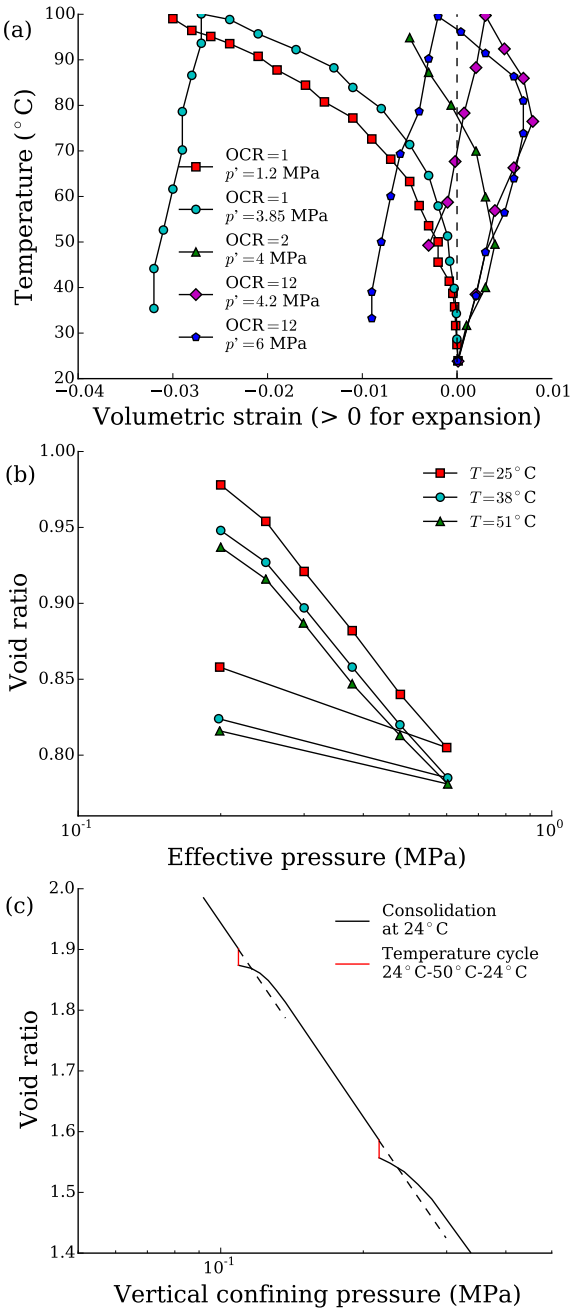

Fig. 1 (a) Drained heating experiments under constant confining pressure, adapted from [48]. (b) Isotropic drained consolidation experiments at different temperatures, adapted from [13]. (c) Effect of temperature cycles on drained consolidation experiments, adapted from [46].

The second experiment (Fig. 1 (b)) is a drained consolidation experiment performed at three different temperatures. The consolidation curves are simply shifted to lower void ratios at higher temperatures. The temperature does not affect the slopes, i.e., the compressibilities, in both the plastic and the elastic regimes. These results were obtained by [13] for illite clay and

similar observations confirmed this observation for kaolin clay [8,16], Todi clay [12], Bangkok clay [3] and bentonite [51].

The last experiment (Fig. 1 (c)) is a drained consolidation under isothermal conditions that has been interrupted twice to perform a heating-cooling cycle. At the beginning of each cycle, the material is normally consolidated. Accordingly, it contracts irreversibly during the cycle. When isothermal consolidation is resumed, it appears that the plastic consolidation occurs at higher pressures than what would have been expected from the consolidation before the temperature cycle (dashed lines). Accordingly, the temperature cycles have increased the preconsolidation pressure and enlarged the elastic domain of the initial temperature. Other experiments reported in the literature investigate the effect of temperature on the elastic domain starting from over consolidated states for which thermal deformations are reversible [53,40,48]: one observes a reduction of the elastic domain with temperature. The interpretation of the experiment of Figure 1 (c) is then as follows: heating leads to a strain hardening of the material because the confining stress is maintained constant while the elastic domain reduces. When the consolidation is resumed, the increase of the elastic domain can be interpreted as a consequence of the thermally-induced strain hardening. Note however, that this last experience is not as consensual as the previous ones: [11] report similar observations as [46], whereas [54] report the same consolidation before and after heating-cooling cycles. Experimental conditions, such as drainage time scales, might explain this discrepancy [12].

The physical origin of the thermo-mechanical behavior of clays is debated and remains unclear. Since thermal contraction disagrees with the thermal expansion of the clay minerals, both in sign and amplitude, one usually attributes the thermo-mechanical behavior to the water filling the porous network. This statement relies on the peculiar state of water in clay. Indeed, for a conventional porous solid in drained conditions, any thermal expansion of the fluid is expected to flow out of the material. According to usual poromechanics [17], the corresponding thermal expansion of a drained porous solid is equal to that of the solid skeleton. However, one of the hypothesis behind usual poromechanics is that the fluid in the pore has the same properties as the bulk fluid. Clays are made of extremely fine grains ($\sim \mu$m or less) which offer a large specific surface on which a large amount of water adsorbs (typically tens of % of all water in saturated clays). A fluid is adsorbed when its constitutive molecules interact with a solid (e.g., electrostatic interactions). The properties of adsorbed water differ strongly from that of bulk water and usual poromechanics does not hold anymore. Water adsorption in clays is well-known to trigger swelling. Since heating induces desorption, one thus expect thermal contraction. This explanation remains very qualitative and, so far, attempts to relate adsorption to the thermal contraction of clays have failed. Early models of adsorbed water in clay consider a continuum fluid with peculiar ionic distribution (diffuse double layer theory) which generates an osmotic pressure different from the bulk water pressure [38]. These models do predict swelling due to low salinity or high humidity. However, when it comes to temperature effects, one expects thermal expansion and not contraction, even when accounting for the change of permittivity with temperature [43]. Application of the double layer theory is indeed questionable when the pores are only a few molecules large, which is the case for consolidated materials. This theory focuses on electrostatics, whereas in very small pores water molecules arrangement is strongly constrained because of short range forces (e.g., steric repulsion) which prevents the development of the diffuse double layer [4]. To sum up, while there is consensus to attribute the complex thermo-mechanical behavior of clays to water adsorption, a proper relationship between the physics of adsorption and the thermo-mechanics of clays is still needed. In particular, some aspects of the thermo-mechanical behavior of clays remain unexplained :

- Adsorption is generally a reversible process. What is the origin of the irreversibility of thermal contractions?
- Why over-consolidation changes radically the thermo-mechanical behavior? How is it related to adsorption?

Since the effect of adsorption is poorly understood, existing engineering models of the thermo-mechanical behavior of clays do not account for nanoscale adsorption. The models are macroscopic only, usually based on an extension of the cam-clay model to account for temperature [30,43,18,26,34]. These models capture experimental observation reasonably well, but their validity beyond experimental results is questionable since the physics of adsorption is not accounted for. In this work, we investigate the physical origin of the thermo-mechanical behavior starting from the scale of adsorption. Recent experimental and theoretical advances in micro- and nano-mechanics of clays offer promising perspectives in the understanding of the mechanical properties (see for instance [1,2]). It is now possible to properly relate the adsorption scale to the macroscopic scale, which is done here for the thermo-mechanical behavior. We use a molecular simulation approach to go beyond

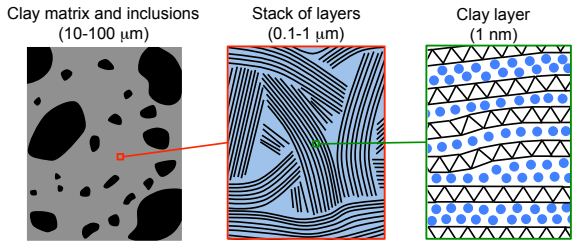

Fig. 2 Schematic representation of the micro- and nanostructure of clays.

usual theories and focus specifically on the structuration of the fluid which dominates the adsorption behavior in slit-like nanopores. We study the effect of temperature on the mechanics of a single nanopore and then propose an upscaling approach to confront with the experimental behavior. We find consistent results for all the key behaviors presented in this introduction. To the best of our knowledge, we propose in this work the first consistent explanation of the physical origin of the thermo-mechanical behavior of clays based on water adsorption. Other physical explanations may exist of course and we do not pretend that our explanation is comprehensive, but this work offers a new look at the fundamentals of clay mechanics.

2 Mechanics at the scale of a clay layer

The elementary constituents of clays are extremely thin minerals layers (~ 1 nm) made of alumino-silicate crystals (Fig. 2). The matrix of clay soils and rock, is made of many of such layers locally stacked together in small particles (a few tenth of layers, ~ 100 nm). At the micrometer scale, such particles are aggregated with some orientational disorder to form a matrix and this matrix is mixed with various mineral inclusions (silica, carbonate) to form a rock. In hydrophilic clays, e.g., smectites, water penetrates and adsorbs between the mineral layers. In geological conditions, the thickness of the water film is less than 2 nm. While the diffuse double layer theory is well suited to describe thick films, it does not hold anymore at such small scales. The arrangement of the fluid molecules is constrained by the slit geometry and a layering of water appears with integer-layers configurations [31]. This peculiar structuration can be observed experimentally by X-ray diffraction [23]. One usually observes up to 2 (possibly 3) water layers (see Fig. 3 (b)). The number of water layers is shown to increase with humidity, thus explaining the humidity-induced swelling. A precise characterization of the mechanical effect of water is extremely hard to obtain experimentally. Experiments of [32] with highly precise surface force apparatus show that the forces exerted by the fluid on the solid oscillates because of the fluid structuration. Alternatively to experiments, molecular simulation studies, relying on the elementary atomic interactions, provide complete strain-stress curves at the layer scale. For convenience, the strain are usually reported through the basal spacing and the stress through the uniaxial pressure in the direction orthogonal to the layer. For instance, we display in Figure 3 (a) typical molecular simulation results of the drained behavior of a Na-montmorillonite layer at ambient water pressure and temperature. In this particular example, there are two oscillations in the curve. Similar curves are available in the literature for other conditions and other types of clay [57,50,14]. A system whose pressure is an increasing function of the basal spacing is unstable. Accordingly, only the decreasing branches of the oscillatory behavior can be observed experimentally. Each decreasing branch corresponds to an integer number of water layers (0 for the first branch, 1 for the second etc.). The example of Figure 3 (a) exhibits 3 decreasing branches, that is 0, 1 and 2 water layers. Therefore, at the layer scale, the mechanical behavior is made of forbidden unstable basal spacings separating authorized (meta)-stable spacings. This is in contrast with the macroscopic scale, where all deformations are possible. Therefore, the transition from the nanoscale to the macroscale is not straightforward and is the focus of the next section.

Before addressing the upscaling methodology, one needs to understand how the behavior of the layer scale evolves with temperature under drained conditions. Interestingly, the effect of temperature has not attracted much attention in the literature so far and only a few results have been reported. The influence of temperature has been studied by X-ray diffraction (see for instance [19,41,23]), but these experiments are performed at controlled humidity in unsaturated conditions, which is therefore not suited for a confrontation with geomechanical experiments (saturated conditions at constant bulk water pressure). Regarding molecular simulation approaches, [52] study the effect of temperature but undrained conditions are considered, which is, again, not adapted. To the best of our knowledge, only [47] report molecular simulation results of the effect of temperature under drained conditions. According to their results, the free energy barrier between stable states (number of water layers) decreases with temperature. The results provided by [47] are limited to free energy and compares two temperatures only. One can derive the confining pressure from the free energy but the derivation is rather inaccurate and difficult to confront with geomechanical experiments.

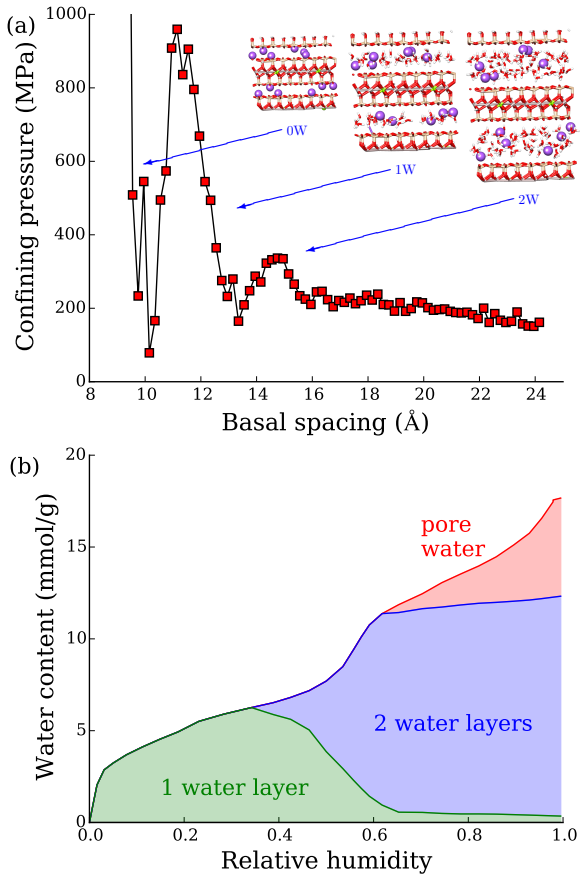

Fig. 3 (a) Typical mechanical behavior at the layer scale in drained conditions obtained by atomistic simulations of Na-Montmorillonite [28]. The inset displays typical configurations associated to no water layer (0W), one water layer (1W) and two water layers (2W). (b) Structuration of pore water evidenced by X-ray diffraction for Na-Montmorillonite [23].

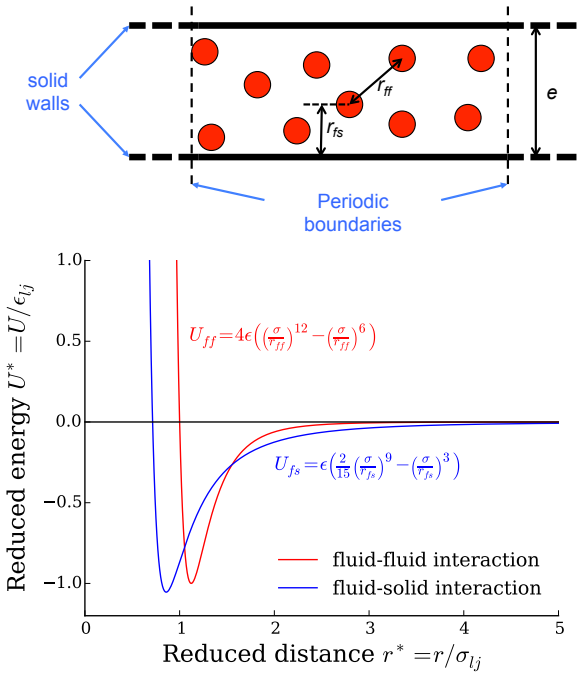

Fig. 4 Toy model considered for molecular simulation study of the effect of temperature on the drained mechanical behavior.

In this section, we report a molecular simulation study of the effect of temperature in saturated drained conditions. For sake of simplicity, we consider a 2D toy model system made of a Lennard-Jones fluid adsorbed between planar solid surfaces (Fig. 4). We deliberately study a very simplistic system to favor accurate results to the detriment of realism. This toy model is one of the simplest system one can imagine that captures the structuration of a fluid film in a flat nanopore. Moreover, a 2D system preserves phase transitions and thus the Lennard-Jones fluid can exist in a liquid state, making it possible to study the saturated drained thermo-mechanical behavior. Of course, real clays are much more complex, but this model is sufficient to capture fluid structuration, which is at the heart of the mechanics of clay layers. In return, the computational cost of the toy model is an order of magnitude smaller than for realistic models of clays, thereby one can assess precisely highly sensitive properties such as thermal expansion.

The interactions between fluid particles is a classical Lennard-Jones potential : $U_{12-6} = 4\epsilon_{lj}\left(\left(\frac{\sigma_{lj}}{r}\right)^{12} - \left(\frac{\sigma_{lj}}{r}\right)^{6}\right)$. The potential is truncated at $r = r_c$. To avoid spurious energy discontinuity at the truncation distance, we consider the shifted potential $U_{ff}(r) = U_{12-6}(r) - U_{12-6}(r_c)$. The interactions between a fluid particle and a solid wall is a 9-3 Lennard-Jones potential, which results from an integration of 12-6 Lennard-Jones interaction over a semi-infinite solid domain of constant density : $U_{9-3} = \epsilon_{lj}\left(\frac{2}{15}\left(\frac{\sigma_{lj}}{r}\right)^{9} - \left(\frac{\sigma_{lj}}{r}\right)^{3}\right)$. The fluid-solid potential is truncated as well and we consider the shifted potential : $U_{fs} = U_{9-3}(r) - U_{9-3}(r_c)$. Note that we use the same Lennard-Jones parameters σ_{lj} and ϵ_{lj} for both the fluid-fluid and the fluid-solid interactions. The simulated systems are with periodic boundary conditions in the direction parallel to the solid wall and with non-periodic boundary conditions in the direction orthogonal to the solid wall. We perform Grand Canonical Monte-Carlo (GCMC) simulations of the Lennard-Jones fluid while controlling the basal distance between the solid walls. GCMC simulations mimic drained conditions since fluid molecules are let in and out to satisfy a prescribed chemical potential of the fluid. All simulations were performed with LAMMPS software package [45] (http://lammps.sandia.gov) with small mod-

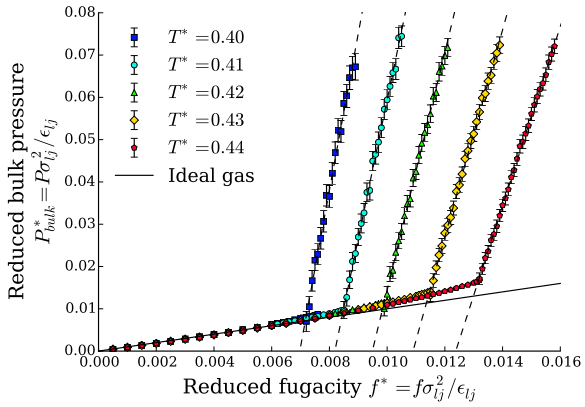

Fig. 5 Pressure of the 2D bulk Lennard-Jones fluid in function of fugacity computed from GCMC simulations at various temperatures. The sudden change of slope corresponds to the gas-liquid phase transition.

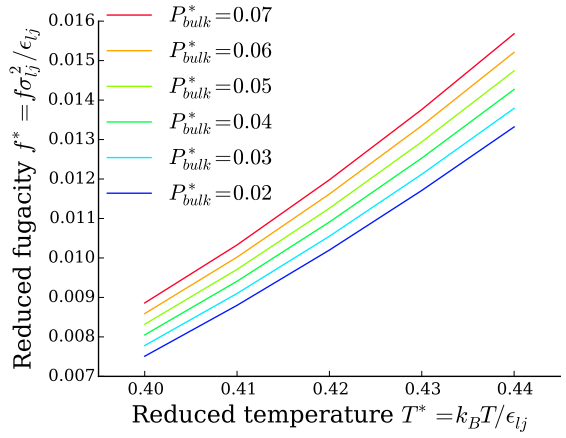

Fig. 6 Temperature-fugacity isobars of the 2D bulk Lennard-Jones fluid. The fluid bulk pressures considered correspond to the liquid phase. These isobars are the input data needed to simulate the toy model in saturated drained conditions.

ifications of the code to enable the use of the fluid-solid 9-3 potential for GCMC simulations. All computations of pressure are obtained with the virial estimate. Hereafter, for sake of generality, all the quantities are reduced to their dimensionless formulation with respect to the Lennard-Jones parameter σ_{lj} and ϵ_{lj}: reduced basal spacing $e^* = e/\sigma_{lj}$, reduced temperature $T^* = k_BT/\epsilon_{lj}$ (k_B is Boltzmann constant), reduced pressure $P^* = P\sigma^2_{lj}/\epsilon_{lj}$.

A preliminary study of the bulk fluid is required to determine its phase diagram and relate the chemical potential to the temperature and bulk pressure for the liquid phase. In 2D, the liquid Lennard-Jones fluid can be observed for reduced temperatures T^* ranging from 0.40 to 0.46. Approaching the critical point (0.46), large fluctuations are detrimental for the accuracy of the simulations. So we limited ourselves to temperatures ranging from $T^* = 0.40$ to $T^* = 0.44$. We perform GCMC simulations of the bulk fluid and compute the pressure P_{bulk} of the fluid in function of the fugacity f. Fugacity is defined with respect to the chemical potential μ according to the relation : $\mu = \mu^0_{IG} + k_BT \ln\left(\frac{f}{k_BT}\right)$, with $\mu^0_{IG} = k_BT \ln\left(\lambda^2\right)$ the chemical potential of an ideal gas at a numeral density of 1 particle per square meter (λ is the thermal de Broglie wavelength). Considering fugacity in GCMC is more convenient than considering chemical potential since the term μ^0_{IG} cancels out in the insertion / deletion probabilities of the Metropolis algorithm [25]. Fugacity has the dimension of a pressure and, therefore, the reduced formulation of fugacity is $f^* = f\sigma^2_{lj}/\epsilon_{lj}$. In Figure 5, we display the fluid bulk pressure in function of the fugacity for various temperatures. The sudden change of slope corresponds to the phase transition from gas at small fugacities to liquid at large fugacities. We also display the case of an ideal gas ($f = P_{bulk}$) as a reference. The saturation points significantly deviate from the ideal gas law for the highest temperatures. The regime we are interested in is the liquid phase. Simulating thermal expansion / contraction of the saturated drained toy model requires to know the fugacity of the fluid in function of the temperature at constant fluid bulk pressure. Such data can be derived from the fugacity-pressure isotherms: we display in Figure 6 the associated temperature-fugacity isobars. The isobars of Figure 6 are used hereafter as input for the toy model simulations.

We then perform GCMC simulations of the toy model for fugacities and temperatures following the isobars of the bulk fluid (Fig. 6). We thus simulate saturated drained conditions. In these simulations, we vary the basal spacing e (here defined as distance between the solid walls) and we compute the average amount of fluid filling the pore and the total pressure P supported by the solid. Because of confinement, the total pressure P differs from the bulk pressure of the fluid P_{bulk}. Several names can be found in the literature for P such as 'solvation pressure' or 'disjoining pressure', which sometimes designate the difference between the total pressure and the bulk fluid pressure. To avoid confusion, in what follows, we will refer to P as to the confining pressure. The results of the GCMC simulations are presented in Figure 7. Figure 7 (a) represents the amount of fluid per unit length of the pore (linear density) in function of the basal spacing. One readily observes that the amount of fluid increases stepwise, each step corresponding to a new layer of fluid filling the pore. The steps are less pronounced for large basal spacing and large temperature. At the highest temperature $T^* = 0.44$, the first 4 to 5 steps are visible. This structuration of the confined fluid is typically ob-

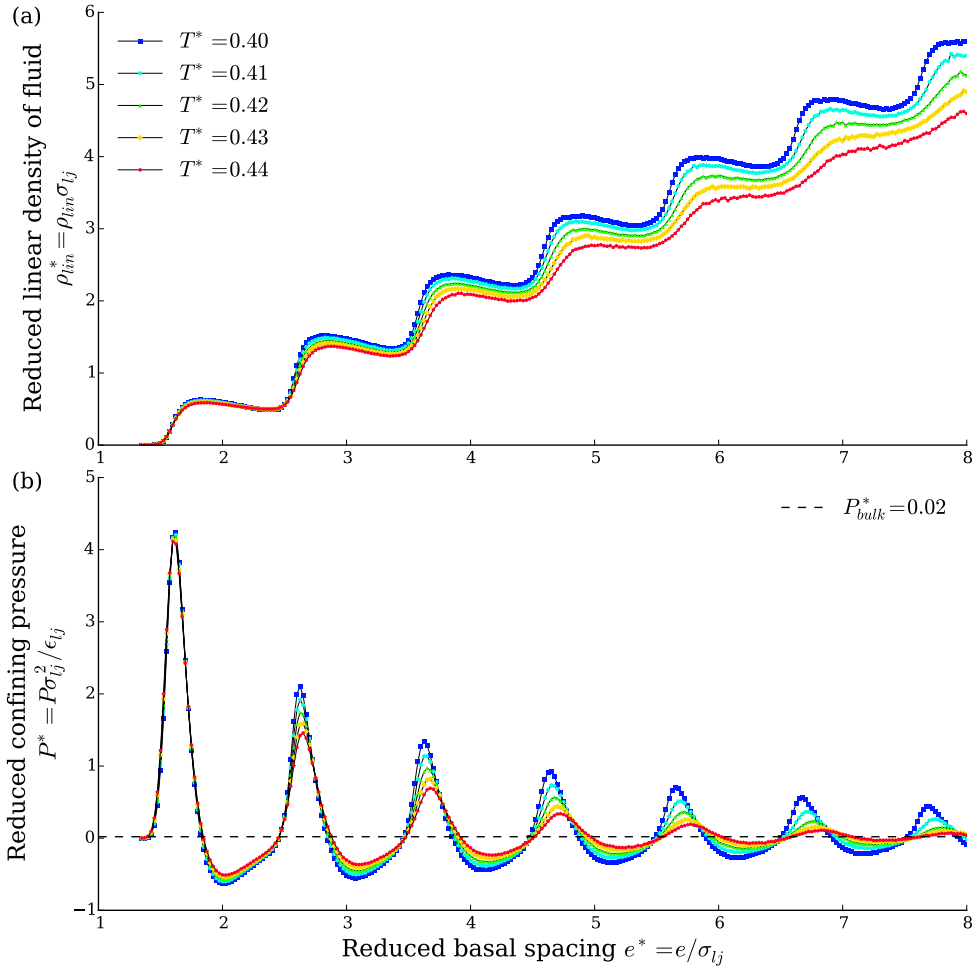

Fig. 7 Results of GCMC simulation of the drained toy model at $P^*_{bulk} = 0.02$. (a) Amount of fluid in function of the basal spacing at various temperatures. (b) Confining pressure in function of the basal spacing.

served in clays, but to a lesser extent (maximum 3 layers, see [37]). Structuration is particularly pronounced for the toy model because the Lennard-Jones fluid can easily adopt semi-crystalline structures, whereas water arrangement in clays is perturbed by the counter-ions. Pure rare gas, which are well modeled with Lennard-Jones fluid, do indeed exhibit strong layering (see for instance the experimental results of [60] which study argon and neon adsorption in graphene: up to 10 layers are observed). Even though, real clays exhibit only a few layers, the theory that we propose hereafter holds as long as at least one layer is present.

As a consequence of fluid structuration, the confining pressure oscillates with respect to the basal spacing (Fig. 7 (b)). Oscillations vanish at large basal spacings and high temperatures. At $T^* = 0.44$, consistently with the density isotherm, only 4 to 5 oscillations can be observed. Proper thermodynamic derivation shows that the confining pressure P is related to the linear density ρ_{lin} according to [10] :

$$P = \int_{-\infty}^{\mu} \left.\frac{\partial \rho_{lin}}{\partial e}\right|_{T,P_{bulk}} d\mu \tag{1}$$

Equation 1 shows that the highest confining pressures correspond to the basal spacings with steep increase of linear density, i.e., to the steps in the density isotherms. Conversely, the lowest confining pressures correspond to basal spacings with decreasing linear density, i.e., in-between two steps. This is indeed what can be observed in Figure 7. An increase of temperature tends to smoothen the linear density isotherm. Accordingly, the amplitude of confining pressure oscillations are decreasing with temperature. Temperature acts as a disordering force.

Another more subtle effect of temperature is that the oscillation peaks are shifted to larger basal spacings upon temperature increase. At a confining pressure equal to the bulk fluid pressure, one can observe that the nanopore expands upon heating. One could

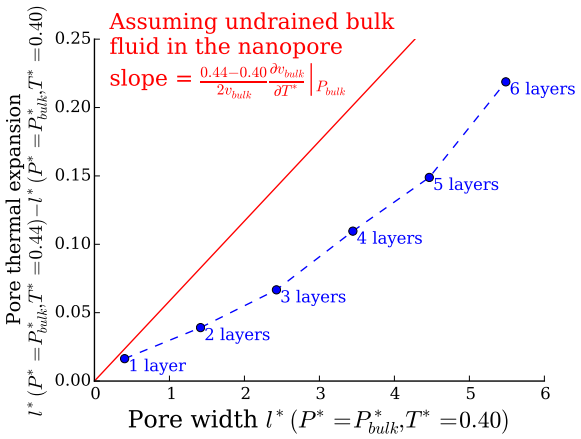

Fig. 8 Thermal expansion of the bulk fluid compared to that of the nanopore maintained at a confining pressure equal to the bulk fluid pressure ($P = P_{bulk}$). The pore width l is estimated from the basal spacing e according to the relation $l = e - 2\sigma_{lj} \cdot \left(\frac{2}{15}\right)^{\frac{1}{6}}$ where the correction arise from the steric repulsion of the 9-3 Lennard-Jones potential of the fluid-solid interactions.

interpret this effect as the thermal expansion of an undrained fluid, insofar as adsorption prevents part of the fluid from leaving the pores ('bound water'). If exactly true, one would expect the following relationship to hold : $\frac{1}{l}\frac{\partial l}{\partial T}\Big|_{P=P_{bulk}} = \frac{1}{v_{bulk}}\frac{2\partial v_{bulk}}{\partial T}\Big|_{P_{bulk}}$, where l is the pore width and v_{bulk} is the molecular volume of the bulk fluid (inverse of the numeral density). The term on the left hand side quantifies the thermal expansion of the solid maintained at a confining stress equal to the bulk fluid pressure; and the term on the right hand side quantifies the thermal expansion of the closed bulk fluid (the factor 1/2 converts a surface thermal expansion into a linear one). This relationship is not strictly verified as shown in Figure 8. At small pore widths (first fluid layers), the thermal expansion of the nanopore is significantly smaller than that of the bulk fluid. At larger pore widths however, the thermal expansion of the nanopore resembles that of the bulk fluid. Discrepancies arise from the fact that the adsorbed fluid is not undrained (part of the fluid is drained upon heating), and the fluid-solid interactions alter the behavior.

In summary, drained heating at the layer scale has two consequences on the mechanics :

1. The amplitudes of the oscillations in the confining pressure isotherm decrease.
2. The oscillations are shifted to larger basal spacings.

3 From the nanoscale to the macroscale : upscaling methodology

In the previous section we have investigated the effect of drained heating at the layer scale. But the link with the macroscopic experiments presented in the introduction is far from obvious. Let us consider for instance the case of a drained heating at constant confining stress (Fig. 1 (a)). This loading applied to the confining pressure isotherm at the layer scale (Fig. 7 (b)) would lead to thermal expansion at small confining pressure (P^* close to P^*_{bulk}) and to thermal contraction at confining pressure close to the oscillation peaks (one fluid layer is drained). This corroborates several aspects of the experiments :

- Both thermal expansion and thermal contraction can be observed.
- Thermal contraction is more likely for large temperature increase.
- The amplitude of contraction is larger than the amplitude of expansion.
- Irreversibility of thermal contractions could be interpreted as hysteresis when changing the number of water layers.

However, the role of over-consolidation is still obscure and no proper confrontation with experiments is possible.

We propose in this section an upscaling methodology inspired from the well-established theory of martensitic transformations in materials such as shape memory alloys (SMA) [7]. SMA are peculiar crystalline materials in which the elementary crystals can exist under various phases depending on the temperature and on the mechanical loading. Which phases are present under given conditions is a problem of energy minimization. We illustrate a simple situation in Figure 9 where we represent schematically the Helmholtz free energy of an SMA crystal in function of the strain for different temperatures. At high temperature, there is a global energy minimum which corresponds to the so-called austenite phase. Upon cooling two other phases becomes more favorable, called martensite. However the stress free strains of the martensite phases differ from that of the austenite phase. In the case of a cooling at fixed strain, one can minimize the total energy by mixing the two martensite phases so that the global strain is preserved. Such mixing is possible only for very peculiar crystallography, which makes SMA so special. Any strain in-between the relaxed strains of the two martensite phases can be reached by varying the fraction of the martensite phases in the microstructure, thus leading to an apparent plastic behavior. Upon heating, the material will invariably transform into the austenite phase

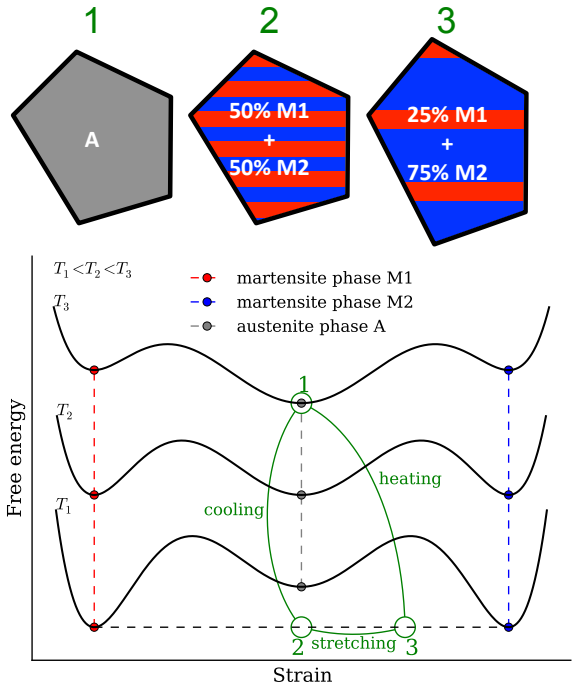

Fig. 9 Schematic representation of the physical mechanism behind the shape memory effect. Different phases of the crystalline structure exists and some can coexists because of peculiar crystallography. The phase composition is dictated by free energy minimization.

and recover the initial strain, hence the 'shape memory' effect.

Interestingly, the physics behind SMA share many similarities with the case of clay. Indeed, at the submicrometer scale clay layers are stacked together in particles of a few tens of layers. Considering that the number of water layers defines a 'phase' of a clay layer, then such stack is analogous to a mix of martensite phases. The overall strain of a stack is a consequence of the respective fractions of the phases. Following the theory of SMA, the mechanics of a stack of clay layers is dictated by energy minimization. For a system in drained conditions, the thermodynamic potential that is minimum at equilibrium is the sum of the Helmholtz free energy of the solid and grand potential of the fluid : $\Lambda = E - TS - \mu_f N_f$, where E is the internal energy, S is the entropy, μ_f is the chemical potential of the fluid and N_f is the number of fluid particles. This energy per unit length of the layer $\lambda = \Lambda/L$ can be obtained by integrating the confining pressure isotherms (Fig. 7 (b)) over the basal spacing :

$$\frac{\partial \lambda}{\partial e} = -P \Rightarrow \lambda\left(e, T, P_{bulk}\right) = -\int_0^e P\left(e, T, P_{bulk}\right) de \tag{2}$$

where we considered the arbitrary reference $\lambda\left(0, T, P_{bulk}\right) = 0$. We display in Figure 10 (bottom) the energy λ in function of the basal spacing e for $T^* = 0.40$. The different local minima correspond to the phases, i.e., integer number of water layers. A stack can mix different phases to minimize the energy, i.e., one follows the 'convex envelop' of the energy isotherm, highlighted in green. The dashed portions of the convex envelop correspond to mixes of two phases. These portions have a constant slope, so the associated confining pressure is constant. The convex envelop of the energy includes all the possible stable states of a stack under displacement-controlled loading. Note that this theory implies that different number of water layers can co-exist within a stack, which is confirmed experimentally [6,24]. The portions of the energy isotherm which are not convex (highlighted in red) are unstable. If an initially homogeneous stack were in such a configuration, it would spontaneously separate in two phases. The remaining portions of the energy isotherm (in blue) are convex but not part of the convex envelop. These are metastable states: a homogeneous stack in such a configuration would not spontaneously separate in two phases, but there exists a heterogeneous stack configuration of lower energy which is more stable. We display in Figure 10 (top) the confining pressure isotherm in which we highlight the stable, unstable and metastable portions with the same color scheme. The most stable mechanical behavior of a stack is the green curve. The phase transitions (dashed) are straights branches at constant pressure which can be interpreted as apparent plasticity.

So far, we have investigated the mechanical behavior of a clay particle, i.e., a stack of clay layers. Above the micrometer scale clay particles arrange with some orientational disorder to form a matrix in which other minerals grains are embedded (silica, carbonate...). Current reconstruction algorithms provide realistic arrangements of particles in the matrix (see for instance [22]). Such reconstructions account for the variability of particle size and shape and their orientational order parameter. Here, for sake of simplicity, we consider conventional homogenization techniques assuming that particles are circular and with random orientations. The motivation of this choice is the same as for the use of the molecular toy model: we favor understanding the physics. Since the thermo-mechanical behaviors presented in introduction holds irrespective of the nature of the clay, even a very basic representation of the microstructure should capture them.

We consider self-consistent homogenization of an heterogeneous material made of elastic circular inclusions in a 2D infinite homogeneous isotropic elastic solid. According to the corresponding Eshelby solution, the

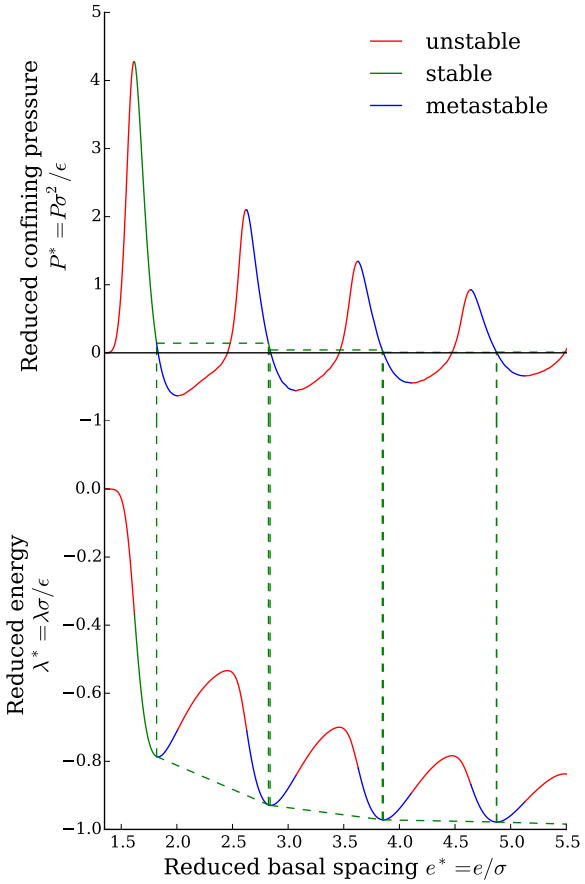

Fig. 10 Application of the theory of martensitic transformations (SMA) to a stack of clay layers. The system minimizes the energy λ. A stack can be a mix of different phases (number of water layers). Accordingly the system follows the convex envelop of the energy (green). Metastable and unstable portions are represented in blue and red, respectively.

Hill's tensor $\mathbb{P}$ for this problem is (derivation from the general 2D solution of [35], or equivalently from the 3D solution of a cylindrical inclusion [27]):

$$\mathbb{P} = \frac{1}{2\left(K+\mu\right)}\mathbb{J} + \frac{K+2\mu}{4\mu\left(K+\mu\right)}\mathbb{K} \tag{3}$$

where $\mathbb{J}$, $\mathbb{K} = \mathbb{I} - \mathbb{J}$ and $\mathbb{I}$ are the unit forth-order spherical, deviatoric and identity tensors: $\mathbb{I}_{ijkl} = \frac{1}{2}(\delta_{ik}\delta_{jl} + \delta_{il}\delta_{jk})$, $\mathbb{J} = \frac{1}{2}\underline{\underline{1}} \otimes \underline{\underline{1}}$[1].

The Hill's tensor relates the local microscopic deformation $\underline{\underline{\varepsilon_I}}$ in the elastic inclusion (elasticity tensor $\mathbb{C}_I$) to the remote macroscopic deformation $\underline{\underline{E}}$ applied to the infinite matrix (elasticity tensor $\mathbb{C}$):

$$\underline{\underline{\varepsilon_I}} = \left(\mathbb{I} + \mathbb{P} : \left(\mathbb{C}_I - \mathbb{C}\right)\right)^{-1} : \underline{\underline{E}} = \mathbb{A} : \underline{\underline{E}} \tag{4}$$

[1] The notation $\otimes$ is defined as $\left(\underline{\underline{a}} \otimes \underline{\underline{b}}\right)_{ijkl} = a_{ij}b_{kl}$

where $\mathbb{A}$ is called the strain localization tensor. In a medium made of many such inclusions, self-consistency requires that the average deformation over all the inclusions equals the macroscopic deformation which leads to a self consistent condition that the homogenized elasticity $\mathbb{C}$ must verify [21]:

$$\mathbb{C} = \overline{\mathbb{C}_I : \mathbb{A}} = \overline{\mathbb{C}_I : \left(\mathbb{I} + \mathbb{P} : \left(\mathbb{C}_I - \mathbb{C}\right)\right)^{-1}} \tag{5}$$

where the notation $\bar{\cdot}$ stands for the space average operator and $\cdot : \cdot$ stands for the double tensor contraction[2]. Here, the homogeneous matrix is isotropic, and, accordingly its elasticity tensor takes the form : $\mathbb{C} = 2K\mathbb{J} + 2\mu\mathbb{K}$, with K the 2D bulk modulus and μ the 2D shear modulus. Regarding the inclusions, these are orthotropic (stacks of layers) with random orientations so that the homogenized medium is isotropic. Considering $\underline{t}$ and $\underline{n}$ the orthogonal directions of orthotropy of an inclusion, its elasticity tensor can be expressed in Voigt notation in this basis :

$$\mathbb{C}_I = \begin{bmatrix} C_{tttt} & C_{ttnn} & 0 \\ C_{ttnn} & C_{nnnn} & 0 \\ 0 & 0 & C_{tntn} \end{bmatrix} \tag{6}$$

where C_{tttt}, C_{nnnn} and C_{tntn} are the transverse, normal and shear elasticities, and C_{ttnn} is the coupling elasticity between the transverse and normal directions. Alternatively, one can decompose this elasticity tensor in a 2D equivalent of the Walpole basis [56]:

$$\mathbb{C}_I = C_{tttt}\mathbb{E}_1 + C_{nnnn}\mathbb{E}_2 + 2C_{tntn}\mathbb{E}_3 + C_{ttnn}\left(\mathbb{E}_4 + \mathbb{E}_5\right) \tag{7}$$

where the $\left(\mathbb{E}_i\right)_{i\in\{1,\dots,5\}}$ are a convenient basis for orthotropic tensors : $\mathbb{E}_1 = \underline{\underline{I_t}} \otimes \underline{\underline{I_t}}$, $\mathbb{E}_2 = \underline{\underline{I_n}} \otimes \underline{\underline{I_n}}$, $\mathbb{E}_3 = \underline{\underline{I_n}} \overline{\otimes} \underline{\underline{I_t}} + \underline{\underline{I_t}} \overline{\otimes} \underline{\underline{I_n}}$[3], $\mathbb{E}_4 = \underline{\underline{I_n}} \otimes \underline{\underline{I_t}}$ and $\mathbb{E}_5 = \underline{\underline{I_t}} \otimes \underline{\underline{I_n}}$, where we used the notation $\underline{\underline{I_t}} = \underline{t} \otimes \underline{t}$ and $\underline{\underline{I_n}} = \underline{n} \otimes \underline{n}$[4]. Usual tensor operations are simplified within this basis : for $i \in \{1,2,3\}$, $\mathbb{E}_i : \mathbb{E}_i = \mathbb{E}_i$, $\mathbb{E}_4 : \mathbb{E}_1 = \mathbb{E}_4$, $\mathbb{E}_4 : \mathbb{E}_5 = \mathbb{E}_2$, $\mathbb{E}_5 : \mathbb{E}_2 = \mathbb{E}_5$, $\mathbb{E}_5 : \mathbb{E}_4 = \mathbb{E}_1$, and all other $\mathbb{E}_i : \mathbb{E}_j = 0$. One can decompose the isotropic unit tensors $\mathbb{I}$, $\mathbb{J}$ and $\mathbb{J}$ as follows $\mathbb{I} = \mathbb{E}_1 + \mathbb{E}_2 + \mathbb{E}_3$, $\mathbb{J} = \frac{1}{2}\left(\mathbb{E}_1 + \mathbb{E}_2 + \mathbb{E}_4 + \mathbb{E}_5\right)$, and $\mathbb{K} = \frac{1}{2}\left(\mathbb{E}_1 + \mathbb{E}_2 + 2\mathbb{E}_3 - \mathbb{E}_4 - \mathbb{E}_5\right)$.

Using this algebra, the right-hand side of Equation 5 is conveniently decomposed as a linear combination

[2] $\left(\mathbb{A} : \mathbb{B}\right)_{ijkl} = \sum_{mn} \mathbb{A}_{ijmn}\mathbb{B}_{mnkl}$

[3] The notation $\overline{\otimes}$ represents a special product defined as follows : $\left(\underline{\underline{a}} \overline{\otimes} \underline{\underline{b}}\right)_{ijkl} = \frac{1}{2}\left(a_{ik}b_{jl} + a_{il}b_{jk}\right)$.

[4] The product $\otimes$ between one dimensional vectors is defined as follows : $\left(\underline{a} \otimes \underline{b}\right)_{ij} = a_i b_j$.

of the averages $\overline{\mathbb{E}_i}$, since averaging is taken over the orientation $(\underline{t}, \underline{n})$ of the orthotropic inclusions and the dependency on orientation is fully accounted for within the $\mathbb{E}_i$. Assuming a uniform distribution over all possible orientations, we obtain : $\overline{\mathbb{E}_1} = \overline{\mathbb{E}_2} = \frac{1}{2}\mathbb{J} + \frac{1}{4}\mathbb{K}$, $\overline{\mathbb{E}_3} = \frac{1}{2}\mathbb{K}$, and $\overline{\mathbb{E}_4} = \overline{\mathbb{E}_5} = \frac{1}{2}\mathbb{J} - \frac{1}{4}\mathbb{K}$. Therefore, the right-hand side of the self-consistent condition equation (Eq. 5) can be decomposed as a linear combination of $\mathbb{J}$ and $\mathbb{K}$. As expected the averaging does lead to an isotropic elasticity, and one ends up with a direct identification of two scalar equations for the $\mathbb{J}$ and $\mathbb{K}$ components, respectively. The self consistent problem is solved numerically with classical algorithms for fixed point search.

Two aspects however require adaptation of the self-consistent homogenization :

1. The mechanical behavior of the inclusions is non linear, so a specific formulation is needed to account for non linearity. Here, we consider an incremental formulation known as Hill's approach [9].
2. Thermal loadings induce pre-stresses / pre-strains that have to be accounted for.

Let us first consider the presence of pre-stresses [58, 44]. The Eshelby solution with pre-stresses is modified and Equation 4 becomes :

$$\underline{\underline{\varepsilon_I}} = \mathbb{A} : \left(\underline{\underline{E}} + \overline{\mathbb{A} : \mathbb{P} : \underline{\underline{\sigma_{I0}}}} - \mathbb{P} : \underline{\underline{\sigma_{I0}}}\right) \tag{8}$$

where σ_{I0} is the pre-stress of the inclusion. The consistency conditions $\overline{\underline{\underline{\varepsilon_I}}} = \underline{\underline{E}}$ leads to the same self-consistent equation (Eq. 5) for the homogenized elasticity. Accordingly, the determination of the homogenized elasticity remains unchanged. In addition, the presence of pre-stresses triggers a macroscopic pre-stress $\underline{\underline{\Sigma_0}} = \overline{\underline{\underline{\sigma_{I0}}} : \mathbb{A}}$, where the strain localization tensor $\mathbb{A}$ is identical to the case without pre-stresses (Eq. 4). In fine, the macroscopic behavior law is :

$$\underline{\underline{\Sigma}} = \mathbb{C} : \underline{\underline{E}} + \underline{\underline{\Sigma_0}} \tag{9}$$

Now, we can consider Hill's incremental formulation of the homogenization [9]. This approach is one of the simplest to account for non linearity, but neglects intraphase fluctuations and thus is known to overestimate the homogenized rigidity. In an inclusion, an increment of stress can arise from an increment of strain, or from an increment of pre-stress because of a change of temperature. Accordingly, the incremental behavior law of an inclusion is: $\underline{\underline{d\sigma_I}} = \mathbb{C}_I : \underline{\underline{d\varepsilon_I}} + \underline{\underline{\alpha}} dT$, where $\underline{\underline{\alpha}} = \left.\frac{\partial \underline{\underline{\sigma_{I0}}}}{\partial T}\right|_{\underline{\underline{\varepsilon_I}}}$ is the thermal rigidity of the inclusion. An incremental homogenization thus provides the following macroscopic behavior law:

$$\underline{\underline{d\Sigma}} = \mathbb{C} : \underline{\underline{dE}} + \underline{\underline{A}} dT \text{ with } \underline{\underline{A}} = \overline{\underline{\underline{\alpha}} : \mathbb{A}} \tag{10}$$

$\underline{\underline{A}}$ is the macroscopic thermal rigidity. To apply this incremental formulation, one has to proceed by small loading increments ($\underline{\underline{dE}}$, dT) and, at each increment, update the values of the microscopic properties $\underline{\underline{\alpha}}$ and $\mathbb{C}_I$. This update requires the update of the local strains which is given by :

$$\underline{\underline{d\varepsilon_I}} = \mathbb{A} : \underline{\underline{dE}} + \mathbb{A} : \overline{\mathbb{A} : \mathbb{P} : \underline{\underline{\alpha}} dT} - \mathbb{A} : \mathbb{P} : \underline{\underline{\alpha}} dT \tag{11}$$

Since many experiments on clays are performed under stress control, one may be interested in an alternative formulation of the homogenization in which $\underline{\underline{\Sigma}}$ is the loading parameter instead of $\underline{\underline{E}}$. In that case, the macroscopic behavior law would be:

$$\underline{\underline{dE}} = \mathbb{S} : \underline{\underline{d\Sigma}} - \underline{\underline{B}} dT \text{ with } \mathbb{S} = \mathbb{C}^{-1} \text{ and } \underline{\underline{B}} = \mathbb{C}^{-1} : \overline{\underline{\underline{\alpha}} : \mathbb{A}} \tag{12}$$

$\mathbb{S}$ is the macroscopic compliance tensor and $\underline{\underline{B}}$ is the macroscopic thermal expansion. The local strains in the inclusion are obtained according to:

$$\underline{\underline{d\varepsilon_I}} = \mathbb{A} : \mathbb{S} : \underline{\underline{d\Sigma}} - \mathbb{A} : \underline{\underline{B}} dT + \mathbb{A} : \overline{\mathbb{A} : \mathbb{P} : \underline{\underline{\alpha}} dT} - \mathbb{A} : \mathbb{P} : \underline{\underline{\alpha}} dT \tag{13}$$

In the application of this upscaling methodology, we limited ourselves to isotropic loadings. Non isotropic loadings would induce different local deformations in the inclusions depending on their orientation, and, because of non linearities, one would loose the symmetry of the microstructure, i.e., the macroscopic medium would not be isotropic anymore. Considering isotropic loadings ensures that all inclusions follow the same evolution irrespective of their orientation.

4 Capturing irreversibilities

In the upscaling methodology we proposed in the previous section, one essential phenomenon is missing: irreversibility. Indeed, with this methodology, the mechanical behavior is fully reversible. The mechanics of a particle is given by the green curve in Figure 10 which is reversible. And the homogenization approach does not introduce any irreversibility. This is inconsistent with experiments which show that irreversibility

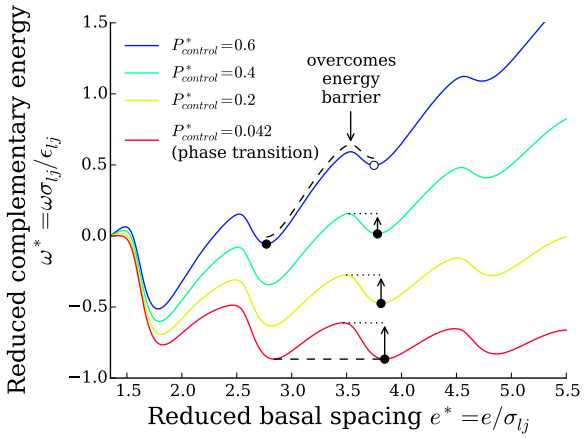

Fig. 11 Energy barrier associated with metastability: case of the transition from 3 fluid layers to 2 fluid layers for the toy model. The energy barrier is the highest when at the pressure of phase transition. The higher the pressure the lower the energy barrier and the more likely it can be overcome (i.e., loss of metastability). In the limit of 0K, all metastable states can exist; and, in the limit of high temperatures, metastability is unlikely.

is at the heart of the thermo-mechanical behavior of clays. Irreversibilities may arise from a wide variety of mechanisms. In shape memory alloys for instance, recent advances attribute hysteresis to the energy barriers due to imperfect interfaces between the austenite and martensite phases [59]. Regarding clays, irreversibility may be due to various mesoscale processes such as rearrangements in the assemblies of particles, but we focus in this work on irreversibilities arising at the nanoscale. Indeed, in Figure 10 we highlight some portions of the confining pressure isotherm which are metastable. These states may be observed even though there exists a (stable) state of lower energy for the same basal spacing. To reach the stable state, the system has to overcome an energy barrier. Metastability is unlikely if the energy barrier is easily overcome by thermal agitation ($k_BT/2$ per degree of freedom). Conversely, metastability is likely if the energy barrier is larger than thermal agitation.

The energy barrier is the energy needed by one clay layer to undergo a phase change. A basic estimate of this energy barrier is obtained by considering the complementary energy $\omega = \lambda - P_{control}e$, characterizing a clay layer maintained at constant pressure $P_{control}$ (for large stacks, a single clay layer is almost under pressure control). In Figure 11, we illustrate, for the 2D toy model, the case of the transition between the 3 fluid layers and 2 fluid layers. When the pressure $P_{control}$ is equal to the phase transition pressure, the two phases have exactly the same complementary energy and the energy barrier in-between is the highest. As $P_{control}$ is increased, one starts to explore metastable configurations of the 3 layers phase. The energy of the 2 layers phase becomes lower and the energy barrier decreases. When the energy barrier is small enough, it is overcome and the metastibility is lost. The energy barriers for our toy model are up to $\omega^* \approx 0.35$. Comparison with thermal agitation gives $\omega/(k_BT) \approx 0.85/\sigma_{lj}$. ω is an energy per unit length. Since any clay layer is orders of magnitude longer than the size of a fluid molecule (σ_{lj}), our toy model is prone to metastability.

Regarding realistic molecular models of clay, some studies in the literature investigate this energy barrier. The complementary energy ω is often referred to as 'swelling energy' in the literature. [50] report values of a few tens of k_BT/nm^2 for various montmorillonites. Since the surface area of clay layers is about 10^3 to 10^5nm^2, the total energy barrier is in favor of metastability. Such a representation of the energy barrier is highly idealized. In reality the phase changes are likely to involve bending of the minerals so that only a small portion of the clay layer needs to overcome the energy barrier (in the spirit of dislocations involved in metal plasticity). Conventional nanometer-scale molecular simulations do not experience any bending, but high performance simulations at the scale of a full clay layer (sub-micrometer) have shown that bending is significant [49]. Moreover additional energy penalties may arise from the peculiar interactions at the extremities of the clay layers. In fine, little can be said about the true energy barriers involved in clays. Assuming that bending of the mineral layers takes place over a dozen of nanometers, the energy barrier would be a few hundreds of k_BT without taking into account the bending energy, which could be significant. Such minimal estimation is clearly in favor of metastability. Finally, let us mention that experimental observations do support the existence of hysteresis at the layer scale (see for instance [55] or [33]).

In our upscaling approach, we include the metastability at the nanoscale. A clay layer does not undergo phase change at the point of phase coexistence but explores the metastable branch of Figure 10 at least in part. Since little is known about the true energy barriers, the point of phase transition has to be chosen arbitrarily somewhere along the metastable branch. Here we consider a threshold κ in complementary energy barrier $\Delta\omega/(k_BT)$ to decide of the point of phase transition: if the complementary energy barrier is smaller or equal to the threshold ($\Delta\omega/(k_BT) \leq \kappa$) then metastability is lost and phase transition occurs. We do not pretend that this choice is fully relevant, but it makes sense with respect to the physics involved and what is currently known of nanoscale metastability. With this

modification of the nanoscale behavior, we keep the same upscaling approach as described previously. The behavior of a stack of layers can be formulated formally as follows:

$$\begin{aligned} & P = -\sum_{i\in\text{phases}} \theta_i \left.\frac{\partial\lambda(e_i)}{\partial e}\right|_{T,P_{bulk}} \\ & \text{and} \\ & \frac{d\theta_i}{dt} = \begin{cases} = -r < 0 & \text{if } \Delta\omega_i/\left(k_B T\right) \leq \kappa \\ \geq 0 & \text{otherwise} \end{cases} \end{aligned} \tag{14}$$

where the subscript i refer to the phases and θ_i is the fraction of phase i in the stack ($\sum_i \theta_i = 1$ and $\forall i, \theta_i \geq 0$). The first equation relates the total confining pressure of a stack to the confining pressures of its constitutive phases. Here, we assume the same confining pressure in all the phases ($\left.\frac{\partial\lambda(e_i)}{\partial e}\right|_{T,P_{bulk}} = \left.\frac{\partial\lambda(e_j)}{\partial e}\right|_{T,P_{bulk}}$), thus giving the closure condition to determine the basal spacings e_i of the different phases. The second equation is the condition for phase change and thus change of the fractions θ_i. The fraction θ_i decreases if the complementary energy criterion is met (there is one criterion for compression and another one for traction). The rate r is arbitrary and has no influence on what follows. When a fraction θ_i is decreasing, the other fractions increase to ensure the consistency condition $\sum_i \theta_i = 1$. Since only two phases can coexist in a stack, no additional condition is needed to fully determine the change of phases.

We represent this mechanical behavior in Figure 12 (a). The mechanics of a stack does not follow the stable branch anymore but can evolve in a domain represented by the shaded area. Phase transition is possible only along the horizontal borders of the domain. Inside the domain, the fractions of the phases are fixed and the mechanical behavior of the stack is a linear combination of the behaviors of its constitutive phases. When phase transition occurs, the stack deforms at constant pressure, thus exhibiting apparent perfect plasticity. In Figure 12 (b), we display the evolution of the domain with temperature. An increase of temperature reduces significantly the confining pressure at phase transition. This is mainly due to the decrease of the oscillation peaks of the confining pressure isotherms. The effect of temperature in the complementary energy criterion (Eq. 14) is almost negligible in this evolution.

To sum up, we discuss in this section the possible origin of irreversibility of clay thermo-mechanics at the layer scale and we proposed a modification of the upscaling approach to account for it. The homogenization technique proposed in the previous section can be applied without modification. In the next section we confront our conceptual model to the known experimental behavior of clays.

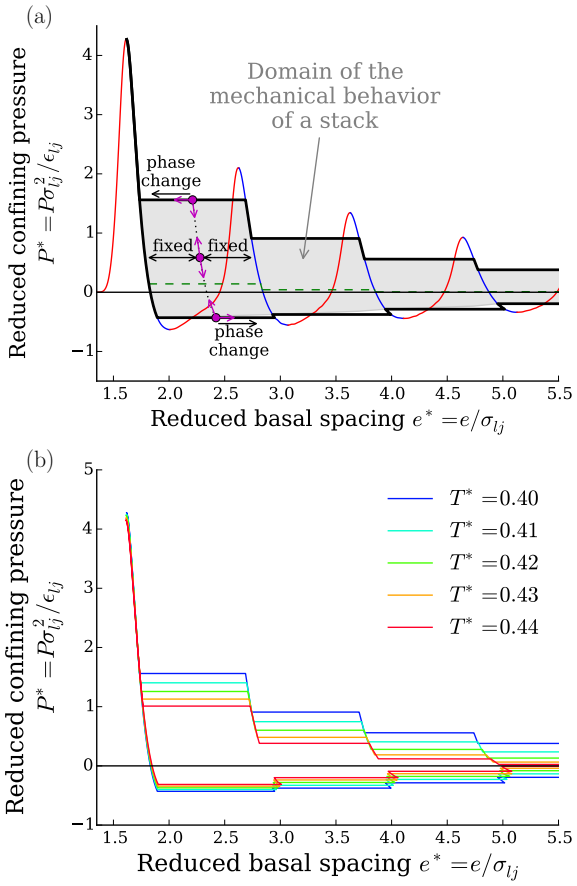

Fig. 12 Mechanical behavior of a stack of layers assuming metastability at the layer scale for $\kappa = 0.1$. (a) The shaded area represents the domain accessible to the mechanical behavior of the stack. Phase transition and variation of the fractions of phases can occur only at the horizontal boundaries of the domain. Inside, the fractions are fixed and the mechanical behavior is a linear combination of that of the phases. (b) Evolution of the domain with temperature.

5 Confrontation with experiments

We apply the approach to typical thermo-mechanical loadings in order to confront with experiments. Let us first precise all the details of the calculations we perform :

- The elementary behavior of a stack of layers is that displayed in Figure 12 (b).
- This behavior provides the values of C_{nnnn} of the elasticity tensor of the inclusions (Eq. 6) : $C_{nnnn} = e\left.\frac{\partial P}{\partial e}\right|_{T,P_{bulk}}$. It also provides the values of the component $\left(\underline{\underline{\alpha}}\right)_{nn}$ of the thermal rigidity of the inclusions.

– The coupling component C_{ttnn} of the elasticity tensor is set to zero since any non zero value would violate the Maxwell relation $\frac{\partial \sigma_{tt}}{\partial \varepsilon_{nn}} = \frac{\partial \sigma_{nn}}{\partial \varepsilon_{tt}}$. This comes from the fact that in our toy system the solid minerals are infinitely thin, and thus cannot exhibit any Poisson effect.
– Linear elastic behavior is assumed for all the other components of the inclusion elasticity: $C^*_{tttt} = C_{tttt}\sigma^2_{lj}/\epsilon_{lj}$ 17.9 (high value corresponding to C_{nnnn} for the 1 fluid layer at $P* = 0$), $C_{tntn} = 0.3 \cdot C_{tttt}$. We deliberately choose a high value for C_{tttt} because the elasticity of clay layers in the transverse direction is governed by the mineral layers and is expected to be higher than in the normal direction [15]. The choice for C_{tntn} is arbitrary and choosing other values does not seem to affect our conclusions.
– The other components of the thermal rigidity are chosen as follows : $\left(\underline{\underline{\alpha}}^*\right)_{tt} = \left(\underline{\underline{\alpha}}\right)_{tt} \sigma^2_{lj}/k_B = 5$ and $\left(\underline{\underline{\alpha}}\right)_{tn} = 0$ (no thermal shear). The value of $\left(\underline{\underline{\alpha}}\right)_{tt}$ corresponds to a thermal expansion ($\mathbb{C}^{-1} : \underline{\underline{\alpha}}$) about 10 times lower than that of the bulk liquid fluid (0.3 vs. 3 in reduced units). We choose this deliberately low thermal expansion because the transverse thermal expansion is governed by the minerals (as for the elasticity), which are known to have thermal expansions about one order of magnitude lower than that of bulk water [36].
– In the homogenization, we consider 50% of inclusions with the properties detailed above, and 50% of isotropic linear elastic inclusions that represent the other minerals in clay rocks (silica, carbonate). The corresponding mechanical properties are chosen as follows : $C^*_{tttt} = C^*_{nnnn} = 17.9$ (same value as the transverse elasticity of the stacks), $C_{ttnn} = 0.4 \cdot C_{nnnn}$ and $C_{tntn} = 0.3 \cdot C_{nnnn}$ (to ensure isotropic elasticity). Regarding the thermal rigidity, we use the same values as for the transverse directions of the stacks : $\left(\underline{\underline{\alpha}}^*\right)_{tt} = \left(\underline{\underline{\alpha}}^*\right)_{nn} = 5$ and $\left(\underline{\underline{\alpha}}\right)_{tn} = 0$.

A preliminary step, necessary before any further investigation of the thermo-mechanics, is to perform consolidation of the material (see Fig. 13). To do so, we consider an initial configuration at large basal spacing and moderate confining pressure. In this initial configuration, all the inclusions have the same initial stress state (spherical stress equal to the confining pressure of a stack). Then, we apply a macroscopic volumetric compression to reach a normally consolidated state (red curve in Fig. 13). Unloading the material produces an over-consolidated material (blue curve). Further loading-unloading cycles follows elastic-plastic cycles which recall that observed experimentally. By restraining ourselves to volumetric loadings and neglecting intra-phase fluctuations in the self consistent homogenization, we impose the same loading to all stacks irrespective of their orientation. Accordingly, for any loading history, there is a single corresponding configuration at the scale of a stack. Thus, any macroscopic mechanical response to consolidation is associated to a specific mechanical response at the scale of a stack, which is displayed in Figure 13 (a). Obviously, intra-phase fluctuations and consolidation with deviatoric loadings would lead to a whole distribution of configurations at the micro scale depending on the orientations of the stacks. But, this simplification offers a particularly convenient interpretation of the macroscopic behavior with a one to one correspondence with the microscopic scale. Regarding consolidation, it appears that macroscopic plasticity arises from microscopic phase transitions, whereas the elastic behavior of over consolidated states is associated with microscopic

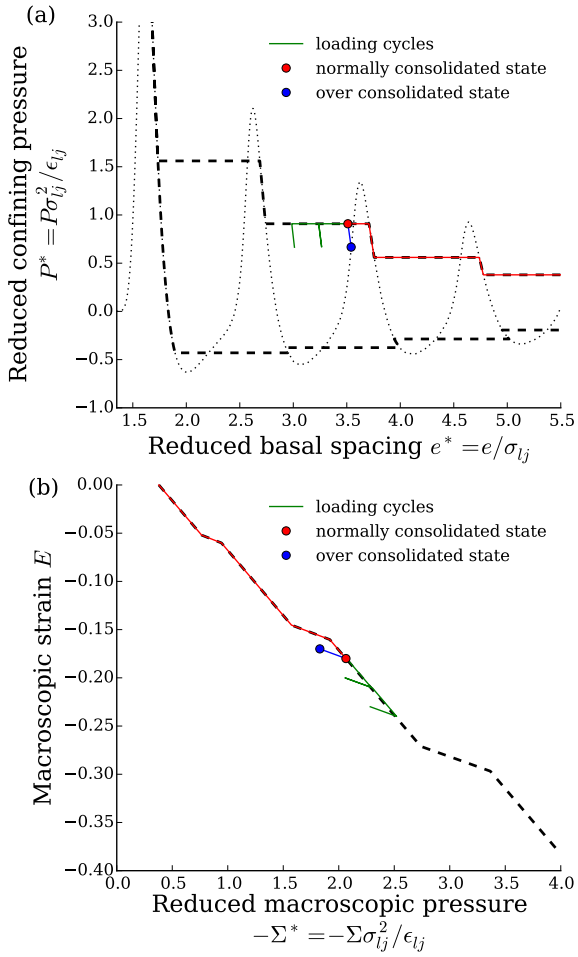

Fig. 13 Consolidation of the material by applying volumetric compression to an initial configuration at large basal spacing and moderate confining pressure. (a) Mechanical response at the scale of a stack. (b) Mechanical response at the macroscopic scale.

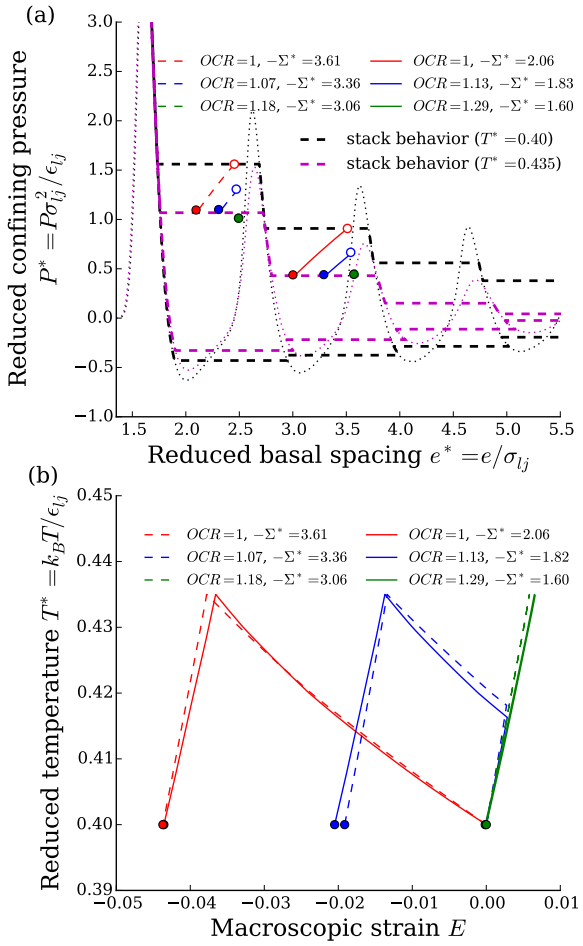

Fig. 14 Mechanical response of the material to an increase-decrease of temperature under constant confining pressure. (a) Mechanical response at the scale of a stack. (b) Deformation in function of the temperature at the macroscopic scale.

response without phase transitions. However, considering all stack orientations identical introduces some spurious consequences such as sudden elastic-plastic transitions, whereas in real clays the transition is usually progressive. Other spurious consequences are the small elastic portions along the consolidation curve, which corresponds to microscopic configurations with a single phase. If orientations were distinguished and microstates distributed over a sufficiently large range of basal spacings, at least some orientations would undergo phase coexistence and irreversibility, and no such reversible portions would appear along the consolidation curve. In what follows, we avoid these elastic portions in our investigations. A more realistic investigation would require to consider homogenization capturing intra-phase fluctuations and deviatoric stresses which differentiate the stack orientations. This is left for future work.

We then apply thermal loading to the normally and over consolidated states of Figure 13 (red and blue dots). We subject those states to a temperature increase and decrease at constant macroscopic pressure as is done in the experiments of Figure 1 (a), and we look at the volumetric deformation induced by this thermal loading. The macroscopic response is displayed in Figure 14 (b) while the corresponding response at the scale of the stack is displayed in Figure 14 (a). Several additional states are considered : one of higher over consolidation ratio, and three others of similar over consolidation ratios but higher confining pressure. These results capture the essential features observed in experiments (Fig. 1 (a)) :

- Normally consolidated materials ($OCR = 1$) exhibit large irreversible contractions upon heating and moderated reversible contractions during cooling. The response is almost insensitive to the confining pressure.
- Moderately over consolidated material ($OCR = 1.13$ for $-\Sigma^* = 1.83$, and $OCR = 1.07$ for $-\Sigma^* = 3.36$) exhibit moderate reversible expansions followed by large irreversible contractions upon heating, and moderate reversible contraction upon cooling. As before, the magnitude of thermal contractions / expansions is almost insensitive to confining pressure. But the transition from expansion to contraction during heating depends on over consolidation ratio and confining pressure. Identical over consolidation ratio but different confining pressures lead to different transition temperature.
- The higher the over consolidation ratio is, the higher the temperature of transition from expansion to contraction. At high over consolidation ratios, the transition is no more observed ($OCR = 1.29$ for $-\Sigma^* = 1.60$, and $OCR = 1.18$ for $-\Sigma^* = 3.06$). The material exhibits only a reversible expansion upon heating, which is recovered during cooling.

All these results are consistent with experimental observations, and find here a possible explanation from the microscale (Fig. 14 (a)): when temperature is increased, the confining pressure of phase transition in a stack decreases. The microstate cannot stay above this limit pressure. So when the limit pressure reaches the microstate, the stack inclusions have to reduce the pressure they support. To maintain a constant macroscopic pressure, load must be transferred to the elastic inclusions (other minerals) which is done by contracting the stack inclusions by mean of irreversible phase transition. A normally consolidated state is initially on the limit pressure, so the material contracts irreversibly as soon as temperature increases. Instead, an over consol-

idated state lies below the limit pressure. So, at the beginning of heating, the mechanical response is reversible. The moderate expansion is due to the fact that the confining pressure isotherm shifts slightly to larger basal spacings, and also because of the conventional thermal expansion of the solid minerals. When the limit pressure reaches the over consolidation state, one observes the same response as for a normally consolidated material. If the over consolidation ratio is large enough, the microstate is still below the limit pressure at the end of the heating. Thus, one only observes moderate reversible expansion. Irrespective of the state considered, when temperature is decreased, the microstate lies always below the limit pressure. So cooling is always associated with moderate reversible contraction. The magnitude (slopes) of macroscopic contractions or expansions are almost insensitive to the confining pressure. This is expected for expansion since the shift of the isotherms increases almost linearly with the basal spacing (Fig. 8) and we considered linear thermal expansion for the minerals. For contraction, this is because the decrease of the phase transition pressure with temperature is almost the same for all the phase transitions (1 layer - 2 layers, 2 layers - 3 layers, etc.). This last observation would require confirmation with realistic molecular simulations of clay layers.

We then consider the loading at different temperatures as investigated in the experiment of Figure 1 (b): a normally consolidated material is heated to four different temperatures under pressure control and then subjected to mechanical loading-unloading. We consider the normally consolidated state of Figure 13. Three additional states are obtained by increasing the temperature at constant confining pressure. The four states are then subjected to identical pressure-controlled loading-unloading. The results are presented in Figure 15. The macroscopic response (b) is consistent with the experimental results (Figure 1 (b)): the mechanical responses at different temperatures are identical but shifted in strain. The higher the temperature is, the lower the strain. As observed experimentally, the temperature does not affect the macroscopic elasticity, be it in the plastic (loading) or elastic (unloading) domain. A look at the mechanical response at the scale of a stack provides a microscopic interpretation of this result (Fig. 15 (a)): the initial heating induces an irreversible contraction since the material is normally consolidated. The resulting states are all normally consolidated at their respective temperatures. Thus, further mechanical loading leads to irreversible phase transition. The corresponding elasticity component transverse to the stack is the same for all temperatures ($C_{nnnn} = 0$), so the macroscopic elasticity is always the same. During

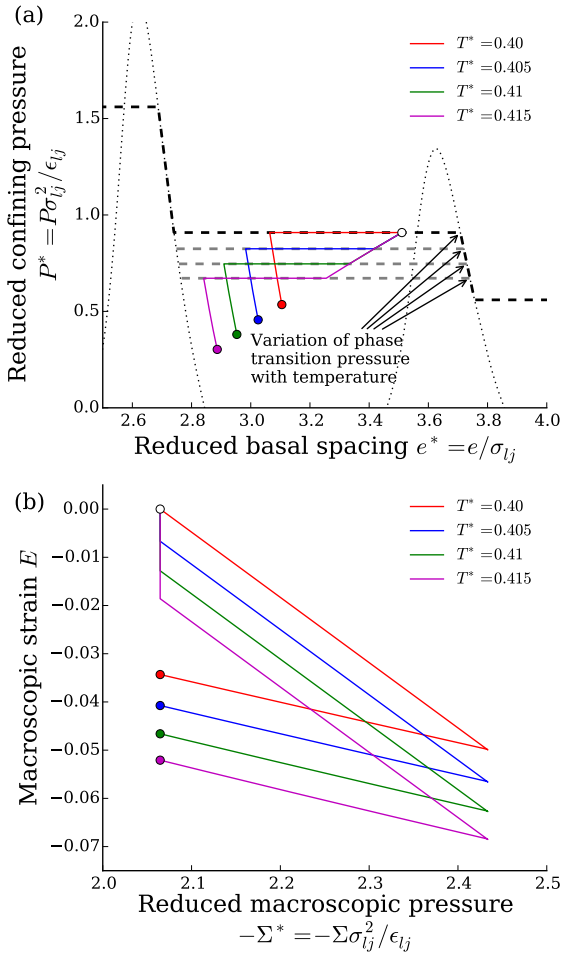

Fig. 15 Normally consolidated material subjected to different temperatures under pressure control, followed by a loading-unloading at these different temperatures. (a) Mechanical response at the scale of a stack. (b) Mechanical response at the macroscopic scale.

unloading, the elasticity are also almost identical (linear combination of the metastable branches), so the same holds for the macroscopic elasticity. As a consequence the initial thermal contraction is preserved all along the mechanical loading-unloading and the macroscopic responses are simply shifted to lower strains.

The last test we perform is a consolidation interrupted by temperature cycles at constant pressure. An experimental result of this test is presented in Figure 1 (c). This result shows an increase of the preconsolidation pressure after the temperature cycle. As mentioned in the introduction, this result is debated, since it is not always observed in the experiments reported in the literature. When applying this test to our model, we do not observe an increase of preconsolidation pressure after a temperature cycle (see Fig. 16 (top)).However, relaxing the condition on the coupling

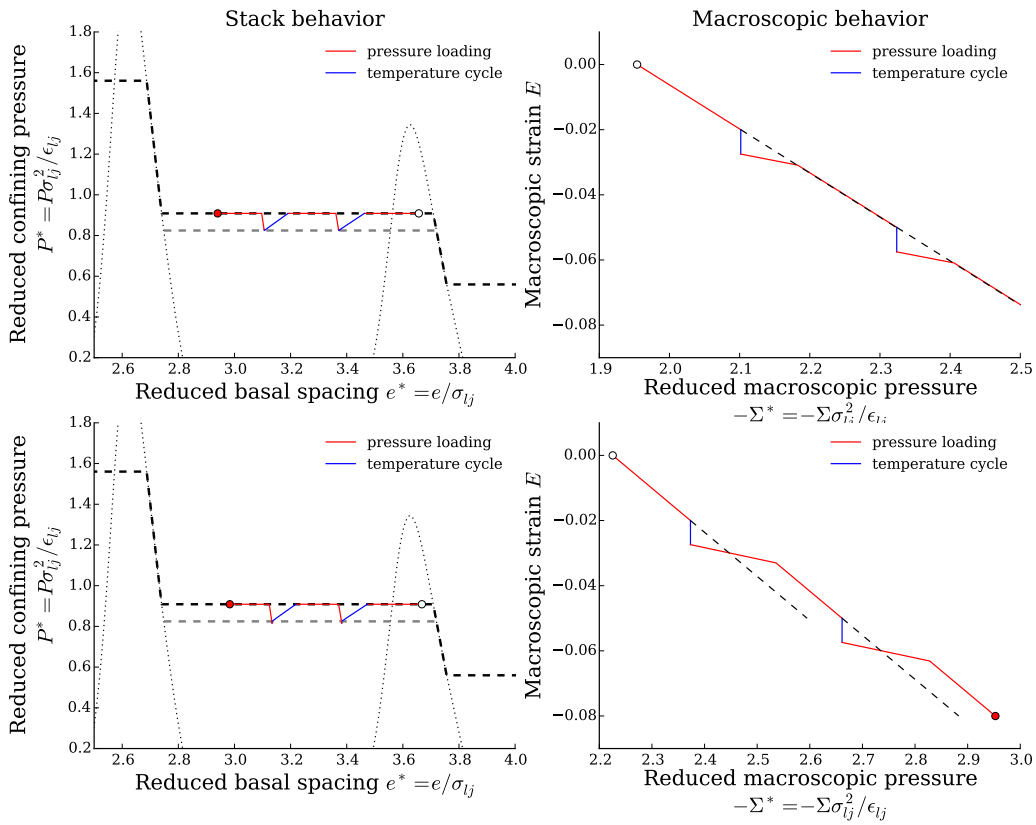

Fig. 16 Consolidation interrupted by temperature cycles at constant confining pressure. Charts at the bottom represent the mechanical response when the elasticity component C_{ttnn} is set to a non zero value: $C_{ttnn} = 0.4C_{nnnn}$. (left) Mechanical response at the scale of a stack. (right) Mechanical response at the macroscopic scale.

coefficient $C_{ttnn} = 0$ and considering a finite value, we do observe an increase of preconsolidation pressure (see Fig. 16 (bottom)). We initially imposed a zero value to C_{ttnn} because we assumed an infinitely thin solid fraction within a layer which means that no Poisson effect is allowed (the stress normal to the layer is a function of the basal spacing only). Of course, this assumption is questionable and we noticed that relaxing it in the present case lead to a clear difference in the macroscopic behavior. When temperature is cycled, part of the load is redistributed between the inclusions and the presence of a Poisson effect plays a role in this redistribution. In Figure 16 (bottom) the choice of C_{ttnn} is arbitrary and does not reflect reality. Actual Poisson effect of clay layers is likely to vary significantly from one clay to another, since the volume fraction of solid mineral is very different from one clay to another (from 100% in a dry clay to 25% or less in highly hydrated states). Accordingly, this could explain why the increase of preconsolidation pressure is not always observed in experiments.

6 Conclusion

In this paper, we propose a physical explanation of the complex thermo-mechanical behavior of clays, based on the effect of adsorption at the scale of clay layers. To do so, we build a conceptual multiscale model articulated in three scales. At the layer scale, the thermo-mechanical behavior of a single drained clay layer is investigated by molecular simulation. The behavior of a clay layer is dominated by the structuration of the interlayer fluid, which gives rise to several possible 'phases' at different ranges of basal spacing. At the particle scale, we build on the theory of martensitic transformations of shape memory alloys to model the mechanics of a stack of clay layers. The mechanics of a stack is governed by energy minimization which allows different phases of clay layers to co-exist within a stack. Metastability and hysteresis of the phase transitions are taken into account as the source of irreversibility. At the scale of the clay matrix and mineral inclusions, conventional self-consistent homogenization is used to estimate the behavior of the macroscopic material from that of a stack of clay layers. This conceptual model captures the main features of the known thermo-mechanical behav-

ior of clays, in particular: thermal expansion or contraction depending on the consolidation history, reversibility or irreversibility of the thermal deformations, effect on the preconsolidation pressure. Three typical tests are investigated and confronted to experimental results representative of a wide variety of clays. Our conceptual model provides consistent results in all cases, and offers interpretations of the macroscopic behavior at the nanoscale. In this conceptual model, the main source of thermo-mechanical coupling is adsorption. To the best of our knowledge, this conceptual model is the first model relating adsorption and the thermo-mechanics clays. Of course, other physical mechanisms may contribute to the thermo-mechanical behavior, but have not been considered in this work.

Acknowledgements We gratefully acknowledge funding from the project TEAM2ClayDesicc from the French National Research Agency (Agence Nationale de la Recherche, contract ANR-14-CE05-0023-01).

References

1. Sara Abedi, Mirna Slim, and Franz-Josef Ulm. Nanomechanics of organic-rich shales: the role of thermal maturity and organic matter content on texture. *Acta Geotechnica*, 11(4):775–787, aug 2016.
2. Y. N. Abousleiman, K. L. Hull, Y. Han, G. Al-Muntasheri, P. Hosemann, S. Parker, and C. B. Howard. The granular and polymer composite nature of kerogen-rich shale. *Acta Geotechnica*, 11(3):573–594, jun 2016.
3. H.M. Abuel-Naga, D.T. Bergado, A. Bouazza, and G.V. Ramana. Volume change behaviour of saturated clays under drained heating conditions: experimental results and constitutive modeling. *Canadian Geotechnical Journal*, 44(8):942–956, aug 2007.
4. G. Baldi, T. Hueckel, A. Peano, and R. Pellegrini. *Developments in modelling of thermo- hydro-geomechanical behaviour of Boom clay and clay-based buffer materials*. Commission of the European Communities, 1991.
5. G Baldi, T Hueckel, and R Pellegrini. Thermal volume changes of the mineralwater system in low-porosity clay soils. *Canadian Geotechnical Journal*, 25(4):807–825, nov 1988.
6. Isabelle Bérend, Jean-maurice Cases, Michèle François, Jean-pierre Uriot, Laurent Michot, Armand Masion, and Fabien Thomas. Mechanism of adsorption and desorption of water vapor by homoionic montmorillonites; 2, The Li+ , Na+ , K+ , Rb+ and Cs+ -exchanged forms. *Clays and Clay Minerals*, 43(3):324–336, 1995.
7. K. Bhattacharya. *Microstructure of martensite: why it forms and how it gives rise to the shape-memory effect*. Oxford University Press, 2003.
8. J. Y. Boisson, J. Billotte, and V. Norotte. *Etude au laboratoire de l'influence de la température sur le fluage des roches argileuses*. Commission des Communautés Européennes, 1993.
9. Michel Bornert, Thierry Bretheau, and Pierre Gilormini, editors. *Homogeneisation en mécanique des matériaux 2. Comportements non linéaires et problèmes ouverts*. Hermes Science, 2001.
10. L. Brochard, M. Vandamme, and R. J M Pellenq. Poromechanics of microporous media. *Journal of the Mechanics and Physics of Solids*, 60(4):606–622, 2012.
11. A. Burghignoli, A. Desideri, and S. Miliziano. Deformability of clays under non isothermal conditions. *Rivista Italiana di Geotecnica*, 4:227, 1992.
12. A. Burghignoli, A. Desideri, and S. Miliziano. Discussion on Volume change of clays induced by heating as observed in consolidation tests. *Soils and Foundations*, 35(3):122–124, 1995.
13. Richard G. Campanella and James K. Mitchell. Influence of Temperature Variations on Soil Behavior. *Journal of the Soil Mechanics and Foundations Division*, 94(3):609–734, 1968.
14. Benoît Carrier. *Influence of water on the short-term and long-term mechanical properties of swelling clays: experiments on self-supporting films and molecular simulations*. PhD thesis, Université Paris Est, 2013.
15. Benoit Carrier, Matthieu Vandamme, Roland J.-M. Pellenq, and Henri Van Damme. Elastic Properties of Swelling Clay Particles at Finite Temperature upon Hydration. *The Journal of Physical Chemistry C*, 118(17):8933–8943, may 2014.
16. Cane Cekerevac and Lyesse Laloui. Experimental study of thermal effects on the mechanical behaviour of a clay. *International Journal for Numerical and Analytical Methods in Geomechanics*, 28(3):209–228, mar 2004.
17. Olivier Coussy. *Mechanics and Physics of Porous Solids*. John Wiley & Sons, Ltd, Chichester, UK, jul 2010.
18. Yu Jun Cui, Nabil Sultan, and Pierre Delage. A thermomechanical model for saturated clays. *Canadian Geotechnical Journal*, 37:607–620, 2000.
19. G J da Silva, J O Fossum, E DiMasi, and K. J. Måløy. Hydration transitions in a nanolayered synthetic silicate: A synchrotron x-ray scattering study. *Physical Review B*, 67(9):094114, mar 2003.
20. Pierre Delage, Nabil Sultan, and Yu Jun Cui. On the thermal consolidation of Boom clay. *Canadian Geotechnical Journal*, 37(2):343–354, apr 2000.
21. Luc Dormieux, Djimédo Kondo, and Franz-Josef Ulm. *Microporomechanics*, volume 1. John Wiley & Sons, Ltd, Chichester, UK, jun 2006.
22. Eric Ferrage, Fabien Hubert, Emmanuel Tertre, Alfred Delville, Laurent J Michot, and Pierre Levitz. Modeling the arrangement of particles in natural swelling-clay porous media using three-dimensional packing of elliptic disks. *Physical Review E*, 91:062210, 2015.
23. Eric Ferrage, Bruno Lanson, Laurent J. Michot, and Jean-Louis Robert. Hydration Properties and Interlayer Organization of Water and Ions in Synthetic Na-Smectite with Tetrahedral Layer Charge. Part 1. Results from X-ray Diffraction Profile Modeling. *The Journal of Physical Chemistry C*, 114(10):4515–4526, mar 2010.
24. Eric Ferrage, Bruno Lanson, Boris A. Sakharov, and Victor A. Drits. Investigation of smectite hydration properties by modeling experimental X-ray diffraction patterns: Part I. Montmorillonite hydration properties. *American Mineralogist*, 90(8-9):1358–1374, aug 2005.
25. Daan Frenkel and Berend Smit. *Undestanding Molecular Simulation: From Algorithms to Applications*. Academic Press, second edition, 2002.
26. J. Graham, N. Tanaka, T. Crilly, and M. Alfaro. Modified Cam-Clay modelling of temperature effects in clays. *Canadian Geotechnical Journal*, 38(3):608–621, 2001.
27. Christian Hellmich, Jean-Francois Barthélémy, and Luc Dormieux. Mineralcollagen interactions in elasticity of

bone ultrastructure a continuum micromechanics approach. *European Journal of Mechanics - A/Solids*, 23(5):783–810, sep 2004.
28. Tulio Honorio, Laurent Brochard, Matthieu Vandamme, Ioannis Stefanou, Siavash Ghabezloo, and Michel Bornert. Stability of hydrated clay layers from molecular simulations. In *paper submitted to Biot conference 2017*, 2017.
29. T. Hueckel and G. Baldi. Thermoplasticity of Saturated Clays: Experimental Constitutive Study. *Journal of Geotechnical Engineering*, 116(12):1778–1796, dec 1990.
30. T. Hueckel and M Borsetto. Thermoplasticity of Saturated Soils and Shales: Constitutive Equations. *Journal of Geotechnical Engineering*, 116(12):1765–1777, dec 1990.
31. Jacob Israelachvili. *Intermolecular & Surface Forces*. Academic Press, second edition, 1992.
32. Jacob N. Israelachvili and Richard M. Pashley. Molecular layering of water at surfaces and origin of repulsive hydration forces. *Nature*, 306(5940):249–250, nov 1983.
33. David A Laird, Chao Shang, and Michael L Thompson. Hysteresis in Crystalline Swelling of Smectites. *Journal of Colloid and Interface Science*, 171(1):240–245, 1995.
34. L. Laloui and C. Cekerevac. Thermo-plasticity of clays : An isotropic yield mechanism. *Computers and Geotechnics*, 30(8):649–660, dec 2003.
35. Renaud Masson. New explicit expressions of the Hill polarization tensor for general anisotropic elastic solids. *International Journal of Solids and Structures*, 45:757–769, 2008.
36. H. A. Mckinstry. Thermal expansion of clay minerals. *American Mineralogist*, 50(1-2):212–222, 1965.
37. Alain Meunier. *Clays*. Springer-Verlag, Berlin/Heidelberg, 2005.
38. James K. Mitchell and Kenichi Soga. *Fundamentals of Soil Behavior*. John Wiley and Sons, 2005.
39. M. Monfared, J. Sulem, P. Delage, and M. Mohajerani. A Laboratory Investigation on Thermal Properties of the Opalinus Claystone. *Rock Mechanics and Rock Engineering*, 44(6):735–747, nov 2011.
40. Lovisa Moritz. Geotechnical properties of clay at elevated temperatures. Technical report, Swedish Geotechnical Institute, 1995.
41. Shoji Morodome and Katsuyuki Kawamura. Swelling Behavior of Na- and Ca-Montmorillonite up to 150C by in situ X-ray Diffraction Experiments. *Clays and Clay Minerals*, 57(2):150–160, apr 2009.
42. Robert E. Paaswell. Temperature Effects on Clay Soil Consolidation. *Journal of the Soil Mechanics and Foundations Division*, 93(3):9–22, 1967.
43. Jean-Marc Picard. *Ecrouissage thermique des argiles saturées : application au stockage des déchets radioactifs*. PhD thesis, Ecole Nationale des Ponts et Chaussées, 1994.
44. B Pichler and C Hellmich. Estimation of Influence Tensors for Eigenstressed Multiphase Elastic Media with Nonaligned Inclusion Phases of Arbitrary Ellipsoidal Shape. *Journal of Engineering Mechanics*, 136(8):1043–1053, 2010.
45. Steve Plimpton. Fast Parallel Algorithms for Short-Range Molecular Dynamics. *Journal of Computational Physics*, 117(1):1–19, mar 1995.
46. R.L. Plum and M.I. Esrig. Some temperature effects on soil compressibility and pore water pressures. *Highway Research Board Special Report*, 103:231–242, 1969.
47. David E. Smith, Yu Wang, A. Chaturvedi, and Heather D. Whitley. Molecular Simulations of the Pressure, Temperature, and Chemical Potential Dependencies of Clay Swelling. *The Journal of Physical Chemistry B*, 110(40):20046–20054, oct 2006.
48. N Sultan, P Delage, and Y J Cui. Temperature effects on the volume change behaviour of Boom clay. *Engineering Geology*, 64(2-3):135–145, 2002.
49. James L. Suter, Peter V. Coveney, H. Chris Greenwell, and Mary-Ann Thyveetil. Large-Scale Molecular Dynamics Study of Montmorillonite Clay: Emergence of Undulatory Fluctuations and Determination of Material Properties. *The Journal of Physical Chemistry C*, 111(23):8248–8259, jun 2007.
50. Tim J. Tambach, Peter G. Bolhuis, Emiel J M Hensen, and Berend Smit. Hysteresis in Clay Swelling Induced by Hydrogen Bonding: Accurate Prediction of Swelling States. *Langmuir*, 22(3):1223–1234, jan 2006.
51. A.-M. Tang, Y.-J. Cui, and Nathalie Barnel. Thermo-mechanical behaviour of a compacted swelling clay. *Géotechnique*, 58(1):45–54, feb 2008.
52. Stephanie L. Teich-McGoldrick, Jeffery A. Greathouse, Carlos F. Jové-Colón, and Randall T. Cygan. Swelling Properties of Montmorillonite and Beidellite Clay Minerals from Molecular Simulation: Comparison of Temperature, Interlayer Cation, and Charge Location Effects. *The Journal of Physical Chemistry C*, 119(36):20880–20891, sep 2015.
53. Marianne Tidfors and Göran Sällfors. Temperature Effect on Preconsolidation Pressure. *Geotechnical Testing Journal*, 12(1):93–97, 1989.
54. Ikuo Towhata, Pisit Kuntiwattanaku, Ichiro Seko, and Kanta Ohishi. Volume Change of Clays Induced by Heating as Observed in Consolidation Tests. *Soils and Foundations*, 33(4):170–183, 1993.
55. N. Wada, D. R. Hines, and S. P. Ahrenkiel. X-ray-diffraction studies of hydration transitions in Na vermiculite. *Physical Review B*, 41(18):12895–12901, jun 1990.
56. L.J. Walpole. Elastic Behavior of Composite Materials: Theoretical Foundations. *Advances in Applied Mechanics*, 21:169–242, 1981.
57. Heather D. Whitley and David E. Smith. Free energy, energy, and entropy of swelling in Cs, Na, and Srmontmorillonite clays. *The Journal of Chemical Physics*, 120(11):5387, 2004.
58. André Zaoui. Continuum Micromechanics: Survey. *Journal of Engineering Mechanics*, 128(8):808–816, 2002.
59. Zhiyong Zhang, Richard D. James, and Stefan Müller. Energy barriers and hysteresis in martensitic phase transformations. *Acta Materialia*, 57(15):4332–4352, sep 2009.
60. Da-Ming Zhu and J. G. Dash. Evolution of multilayer Ar and Ne films from two-dimensional to bulk behavior. *Physical Review B*, 38(16):11673–11687, dec 1988.